Slow invasion of a fluid from multiple inlet sources in a thin porous layer:Influence of trapping and wettability

Loïc Ceballos, Marc Prat

Slow invasion of a fluid from multiple inlet sources in a thin porous layer: Influence of trapping and wettability

L. Ceballos and M. Prat*
Université de Toulouse, INPT, UPS; IMFT, Avenue Camille Soula, 31400 Toulouse, France and CNRS, IMFT, 31400 Toulouse, France

We study numerically the process of quasistatic invasion of a fluid in thin porous layers from multiple inlet injection sources focusing on the effect of trapping or mixed wettability, that is, when hydrophobic and hydrophilic pores coexist in the system. Two flow scenarios are considered. In the first one, referred to as the sequential scenario, the injection bonds at the inlet are activated one after the other. In the second one, referred to as the kinetic scenario, the injection bonds at the inlet are activated simultaneously. In contrast with the case of purely hydrophobic systems with no trapping, studied in a previous work, it is shown that the invasion pattern and the breakthrough point statistics at the end of the displacement depend on the flow scenario when trapping or mixed wettability effects are taken into account. The transport properties of the defending phase are also studied and it is shown that a one-to-one relationship between the overall diffusive conductance and the mean saturation cannot be expected in a thin system. In contrast with thick systems, the diffusive conductance also depends on the thickness when the system is thin. After consideration of various generic aspects characterizing thin porous systems, the main results are briefly discussed in relation with the water management problem in proton exchange membrane fuel cells.

I. INTRODUCTION

This article is the continuation of the study of slow immiscible displacements initiated in [1]. As in [1], we consider the process of quasistatic invasion of a fluid from multiple inlet injection sources in a porous layer. As discussed in more depth in [1], a first key aspect is that the porous medium can be thin, which means here a thickness of a few mean pore sizes only. A second key aspect is the multiple inlet injection condition, which, as explained in [1], is different from the traditional boundary condition, e.g., [2]. The traditional boundary condition essentially assumes that the inlet is in contact with an invading fluid layer at uniform pressure, whereas we consider the situation where the invading fluid can enter the system at the inlet from multiple independent injection points. As shown in [1], this has a great impact on the organization of the fluid within the porous medium. For a quasistatic displacement, the traditional boundary condition leads always (i.e., whatever the porous medium thickness), to only one breakthrough point at the outlet (breakthrough is when the invading fluid forms a percolating cluster across the porous medium), whereas the multiple injection condition can lead to several breakthrough points, at least when the porous medium is sufficiently "thin" [1].

For the sake of brevity, the motivations for considering thin porous layers and the multiple injection condition will not be repeated here. One can refer to [1]. In the present article, the effect of two distinguishing ingredients is studied: (i) the possible trapping of the defending phase; (ii) the fact that the porous microstructure can be of mixed wettability, which means that hydrophilic and hydrophobic pores can coexist within the porous medium. For simplicity, we implicitly assume that the invading fluid is water. Thus a subregion of the system will be called "hydrophobic" when the displacing fluid is nonwetting and the defending fluid is wetting and will be called "hydrophilic" in the opposite case (displacement of a nonwetting fluid by a wetting fluid). Note however that trapping and mixed wettability effects will not be considered together. For simplicity, the layer will be hydrophobic when trapping is considered. When the effect of mixed wettability is studied, trapping will be ignored.

Trapping can occur when a cluster of the defending phase becomes completely surrounded by the invading phase. In the quasistatic limit considered here, such a cluster cannot be invaded since the pressure is uniform along its boundary at any time unless this cluster is connected to the outlet through a defending fluid subnetwork associated with the presence of the defending fluid in the corners and crevices of the pore space, e.g., [3] for more details. For simplicity, trapping was neglected in [1]. Taking into account trapping requires identifying the trapped clusters, which makes the computations more complicated.

Another aspect lies in the wettability of the medium. In [1], it was assumed that the displaced fluid was wetting whereas the displacing fluid was nonwetting. As discussed in [1] (see also Sec. V of the present article), our motivation for the study of thin systems comes in part from the study of two-phase flows in the so-called gas diffusion layer (GDL) of proton exchange membrane fuel cells (PEMFCs). Although the question is still a subject of debate (e.g., see Ref. [4], and references therein) it is widely considered that the GDL is not uniformly hydrophobic but rather a porous system in which hydrophilic and hydrophobic zones coexist. Such a system is referred to as a system of mixed wettability. Porous systems of mixed wettability are common in other applications, such as soil physics [5] or petroleum engineering [6], for example. Thus, the study of the effect of a mixed wettability is of general interest.

In [1], we introduced two flow scenarios for studying the quasistatic invasion of a nonwetting fluid in a porous layer with multiple injection sources at the inlet, referred to as the sequential and the kinetic scenarios, respectively. In the sequential scenario, the injection bonds at the inlet are activated one after the other. In the kinetic scenario,

*Corresponding author: mprat@imft.fr

the injection bonds at the inlet are activated simultaneously. Details on these scenarios are recalled in Sec. II. In particular, it was shown that the two scenarios lead to the same results as regards the fluid distribution at the end of displacement. This was for hydrophobic systems with no trapping. Interestingly, we shall see that this does not hold anymore when trapping or mixed wettability effects are taken into account.

Another aspect concerns the definition of a thin system. From the breakthrough point statistics as a function of system thickness reported in [1] ultrathin layers were defined as the systems of thickness typically less than about 10–15 lattice spacing units. For thicker systems, it was found that the probability of a pore to be a breakthrough pore scales as l^{d-1} where l is the system thickness and d is the space dimensionality. Thus the number of breakthrough points is scale dependent when the system is thin. This is in contrast with thick systems for which there was only one breakthrough point independent of the system thickness. Although a similar qualitative behavior is found when trapping or mixed wettabily is considered, the results are quantitatively different: The exponent of the power law region is different as well as the size marking the limit between the ultrathin (defined as in [1] as the systems sufficiently thin for not being described by a power law) and thin systems. This clearly indicates that the definition of a thin system is process dependent and cannot be defined intrinsically.

As in [1], we focus on the characterization of the breakthrough point statistics and the pore occupancy (saturation) by the two fluids. As pointed out in [1], breakthrough points correspond to the formation of droplets at the outlet surface of the system and this is one of the few observables in thin systems. In addition, we also characterize the conductivity properties of the defending phase. As discussed in more detail in Sec. V, this is important in relation with the study of GDL. In the context of the present paper, this allows us to better assess the influence of trapping or mixed wettability. The conductivity properties of the defending phase were not studied in [1].

The study is based on pore network (PN) simulations (see Sec. II). Direct simulations of invasion using techniques such as the lattice-Boltzmann method, for example, are possible but only for a very limited number of realizations and rather small networks. It would be actually impossible to obtain the numerous results presented in the paper from direct simulations because of the high computational cost of direct simulations, much higher than the computational cost of PN simulations, e.g., [7].

The paper is organized as follows. The flow scenarios and the corresponding invasion algorithms are presented in Sec. II. Section III is devoted to the study of the effect of trapping in fully hydrophobic systems. The influence of a mixed wettability (without trapping) is studied in Sec. IV. Implications of the results for PEMFC are briefly discussed in Sec. V. We close in Sec. VI by offering a brief discussion on thin systems and some concluding remarks.

II. FLOW SCENARIOS AND INVASION ALGORITHMS

A. Flow scenarios

As in [1], we study the quasistatic immiscible displacement of a defending fluid by a displacing one in a porous layer.

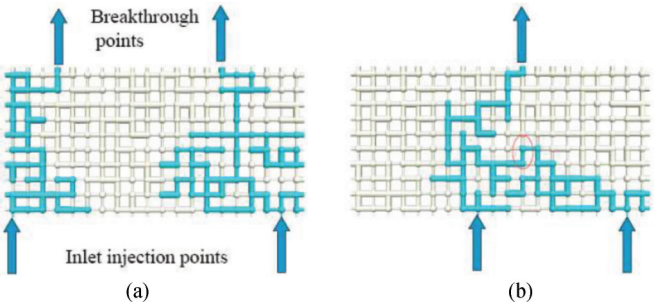

FIG. 1. (Color online) (a) Two distinct breakthrough points are obtained when the displacing fluid is injected in a thin system from two inlet injection points sufficiently far apart; (b) the invasion paths originating from two distinct inlet injection points can merge. The bond in the circle is the one leading to coalescence of the two invasion paths. The invasion path coalescence process leads to a unique breakthrough point in this example. When trapping is perfect the bond in the circle cannot be invaded.

In contrast with most previous studies, the displacing fluid is injected at the inlet through a series of independent entry points. As illustrated in Fig. 1 for the case of two injections, the injection entry points are individual channels at the inlet. These injection channels are called injection bonds; see Sec. II B below. A bond (channel) at the inlet is an active bond when it is an injection bond. An inlet bond is inactive when this is not the case. Two injection bonds are active in the examples shown in Fig. 1. When all bonds are active at the inlet, the fraction of active bonds at the inlet is equal to 100%. The fraction of active bonds at the inlet is a parameter of the study and will be varied. The flow rate q imposed in each active injection bond can vary in space (from one injection bond to the other) and in time *a priori*.

Assuming negligible pressure variations due to viscous effects, the displacement is considered as quasistatic and is therefore controlled by capillary effects only. The invading fluid originating from one active injection bond thus takes the path of least capillary resistance.

Two distinct invasion scenarios are compared. In the first one, the active bonds are activated one after the other. The invasion from an active bond stops when the invading fluid originating from the considered active injection bond percolates through the layer. This scenario corresponds to the sequential algorithm presented below. In the second scenario, which corresponds to the kinetic algorithm below, all active bonds are activated together at the same time. The situation in the applications can be thought of as intermediate between the two scenarios.

Both flow scenarios lead to the formation of flow paths originating from the active inlet bonds. A crucial point is that two flow paths originating from two different active inlet bonds can merge. This is illustrated in Fig. 1. Merging between flow paths can occur in fact repeatedly across the porous layer during the invasion process. The flow path merging phenomenon explains why the number of breakthrough points is less than the number of injection points. The probability of flow path convergence can be expected to increase with the porous layer thickness. As a result, it is expected that the thicker the porous layer, the fewer breakthrough points.

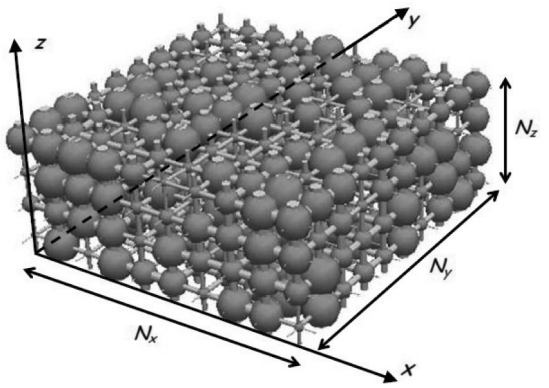

FIG. 2. Sketch of pore network model.

The variation of the number of breakthrough points as a function of system size is studied numerically in what follows using a pore network representation of the porous layer.

B. Pore network

As sketched in Fig. 2, the pore space is conceptualized as a simple regular cubic network (except for the computations of a few phase distributions easier to show in a two-dimensional square network) of randomly sized pores (sites) joined by randomly sized throats (bonds). The distance a between two adjacent pores, referred to as the lattice spacing, is constant. The bonds are straight channels of circular cross section. To each bond a diameter w_b is assigned randomly in the range $[w_{b\min}, w_{b\max}]$ according to a uniform distribution law. The sites (pores) are cubes of side length w_p. The side length w_p of each pore is assigned randomly in the range $[w_{p\min}, w_{p\max}]$ according to a uniform distribution law. The constraint that a pore is larger than the adjacent bonds is imposed, hence $w_{p\min} > w_{b\max}$. The length l of a bond is given by $l = a - 0.5w_{pi} - 0.5w_{pj}$, where w_{pi} and w_{pj} are the side length of the pores adjacent to the bond. The size of the porous network is $L \times L \times W$, where W is the porous medium thickness. Expressed in number of pores along each direction of a Cartesian coordinate system, the size of the network is denoted by $N_x \times N_y \times N_z$ (note that $N_y = N_x$ throughout this paper). The maximum number of possible injection points at the inlet is therefore $N_x \times N_y$. The number of injection points is denoted by N_i and can therefore be varied between 1 and $N_x \times N_y$. As sketched in Fig. 1, the injections are performed through the active bonds located at the pore network inlet.

Spatial periodicity boundary conditions are imposed along the x and y directions, i.e., on the lateral sides of the network (see Fig. 2). The inlet is at $z = 0$, the outlet at $z = W$. The main direction of the flow is therefore the z direction.

N_i is the number of active injection bonds at the inlet. Thus $N_i = N_x^2$ when all inlet bonds are active injection bonds. The probability that an inlet bond is active is denoted by n_i; thus $n_i = N_i/N_x^2$.

C. Quasistatic invasion algorithms

An invasion potential is assigned to each element, pore or throat, in the network. The definition of invasion potential of a pore depends on the wettability of the pore. The classic and simpler case is when a nonwetting fluid displaces a wetting fluid (a process classically referred to as drainage). In this case, the invasion potential ϕ of an element can be defined as $\phi = -2a\cos\theta/w$, where θ is the contact angle ($\theta > 90^\circ$ in a hydrophobic system), where w is the size of the element (we recall that according to Laplace's law, the invasion capillary pressure threshold of a pore or a throat is inversely proportional to its size, thus the larger the element the lower its capillary pressure threshold) and the displacement can be computed using the classical invasion percolation (IP) algorithm [2]. For completeness, we first recall the IP algorithm. At each step of invasion, only one element is invaded: the element of smallest potential (that is, of largest size) available along the interface between the two fluids. When trapping is considered, a throat or a pore that is trapped cannot be invaded. The modeling of trapping is presented in Sec. II D. The algorithm can be readily extended to more complex displacements provided that the invasion potential of each element in the network is adequately defined. This invasion algorithm, which consists in invading the element of smallest potential available along the interface of the considered growing cluster, is referred to hereafter as the quasistatic (QS) algorithm. The case of systems of mixed wettability is considered in Sec. II E. The multiple injection boundary condition at the inlet is dealt with in the sequential and kinetic algorithms, which are summarized below.

1. Sequential algorithm

The sequential algorithm can be summarized as follows [1]:

(1) The network is fully saturated by the wetting fluid initially.

(2) The displacing fluid flow path is computed using the QS algorithm without trapping as in [1] or with trapping (see below) starting from a first injection point. The computation of this step stops at breakthrough, that is, when the invading fluid reaches the outlet.

(3) The simulation is repeated starting from a second active inlet bond. This second invasion stops when one of the two following events occurs: merging or breakthrough. Merging is when the flow path generated from this second injection point merges into the flow path associated with the first inlet injection bond (flow path coalescence). Breakthrough is when the liquid injected from the second inlet bond reaches the outlet through a path independent from the path connected to the first injection point (see Fig. 1).

(4) The procedure is repeated starting successively from all the other active inlet bonds at the inlet. Note that the successive injection points at the inlet can be selected at random among the inlet active bonds or according to a chosen order.

As discussed in [1], two flow paths originating from two distinct injection points can merge. This is illustrated in Fig. 1. In [1], we assumed perfect coalescence, i.e., when a throat on a given flow path is invaded and this throat is adjacent to a pore already invaded, i.e., belonging to an already existing flow path, merging of the two flow paths systematically occurs. However, the coalescence of two flow paths might not systematically occur due to trapping of the wetting fluid in the bond giving access to a flow path previously created. This is discussed in more detail in Sec. II D.

2. *Kinetic algorithm*

In the sequential algorithm the active bonds at the inlet are activated one after the other. With the kinetic algorithm, the active bonds at the inlet are activated simultaneously. Suppose that the injection volumetric flow rate in the ith active inlet bond is q_i. Denoting by m the number of invading fluid clusters present in the network at a given step of the invasion, the kinetic invasion algorithm in the quasistatic limit can be summarized as follows [1]:

(1) Select the element (throat or pore) to be invaded according to the QS rule (element of smallest potential) at the boundary of each invading fluid cluster present in the system. Thus m elements are identified in this step.

(2) Compute the filling time $\delta t_j = \frac{V_w(t)}{\sum q_i}$ of each element selected in step 1, where $V_w(t)$ is the volume of fluid remaining to displace in the element detected in step 1 associated with the jth invading fluid cluster. $\sum q_i$ is the sum of injection flow rates through the active inlet bonds connected to the considered cluster. Note that a growing invading fluid cluster can be connected to several injection points owing to the merging phenomenon. Thus m filling times are computed in this step.

(3) Define as time step $\Delta t = \min(\delta t_j)$. The element corresponding to $\min(\delta t_j)$ is fully invaded; the volume of displaced fluid in each of the $(m-1)$ other elements selected in step 1 is updated as $V_w(t + \Delta t) = V_w(t) - (\sum q_i)\Delta t$.

(4) Update the time, $t = t + \Delta t$, update phase distribution (check for flow paths coalescence and update m), and return to step 1 until all invading fluid clusters present in the system have reached breakthrough.

An interesting distinguishing feature introduced with the kinetic algorithm is that the invasion becomes time dependent. This is in contrast with the sequential algorithm which only describes a succession of phase distributions without any explicit time scale. Intermediate stages of the invasion process can be quite different depending on the algorithm used. However, as explained and shown in [1], the kinetic algorithm and the sequential algorithm lead to the same fluid distribution in the network at the end of invasion in the absence of trapping in a fully hydrophobic layer. As mentioned before and shown below, this does not hold anymore when trapping or a mixed wettability layer is considered. In the following the kinetic algorithm is used assuming that all active (injection) bonds see the same injection flow rate.

D. Trapping

As mentioned before, the influence of trapping phenomena is studied assuming that the porous layer is hydrophobic. The case of trapping in mixed wettability systems is not studied in this article.

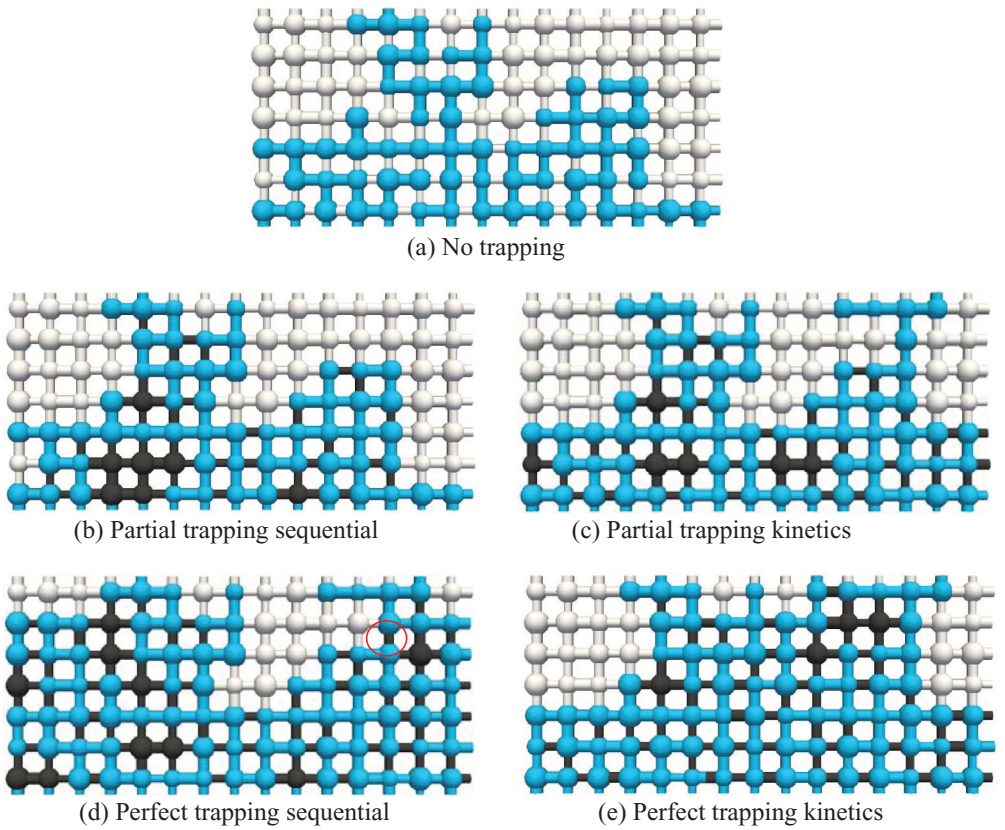

FIG. 3. (Color online) Illustration of trapping. Computed invasion patterns in a small two-dimensional network. Invading fluid in gray (blue online), defending fluid in white. The trapped pores and bonds are dark. The small circle (red online) in Fig. 3(d) shows an example of a trapped bond. The injection is from all inlet bonds. Because of trapping some inlet bonds can become inactive [fourth and fifth inlet bonds from the left in Fig. 3(b), for example]. The breakthrough points correspond to the outlet bonds in gray (blue online). Trapping affects the pattern and the number of breakthrough points [1, 1, 2, 2, and 3 for 3(a), 3(b), 3(c), 3(d), and 3(e), respectively]. The pattern and the number of breakthrough points also depend on the flow scenario, either kinetics or sequential (see text).

As mentioned before, trapping of a pore or bond occupied by the defending fluid occurs when this element (pore or bond) is not connected anymore to the outlet through a path of connected pores and bonds occupied by the defending phase. As a result of invasion by the invading fluid, defending fluid clusters of different sizes can be trapped. We distinguish and compare three cases: no trapping (as in [1]), partial trapping, and perfect trapping. In the absence of trapping, any pore or bond adjacent to a pore occupied by the invading phase can be invaded. With trapping, the trapped pores or bonds cannot be invaded. The difference between perfect and partial trapping lies in the status of a bond of defending phase located between two pores occupied by the invading phase. This is illustrated in Fig. 3 [as for Fig. 1, a two-dimensional (2D) square network is considered for the sake of clarity instead of a cubic network]. Such a bond can be invaded when trapping is partial but cannot when the trapping is perfect. In systems where the bonds correspond to relatively long channels of the pore space, perfect trapping is likely whereas partial trapping is expected when the length of a bond is small compared to the size of adjacent pores (this is the case *a priori* in fibrous materials of high porosity, for example).

As a result, coalescence between flow paths cannot occur with the sequential algorithm when trapping is perfect and the system is hydrophobic since coalescence occurs as the result of the invasion of a bond of the defending phase connecting two flow paths. This corresponds to a coalescence probability of zero (the coalescence probability is 1 when trapping is ignored as in [1]). However, coalescence is still possible with the kinetic algorithm through the mechanism of coalescence in a pore (two independent flow paths feed the same pore in the invading fluid). Pore coalescence cannot occur with the sequential algorithm because a pore is never partially invaded with this algorithm. Thus contrary to the situation without trapping, it is clear that the sequential algorithm and the kinetic algorithm will not lead to the same results in the presence of trapping phenomena.

It could be tempting to conclude that the sequential algorithm with perfect trapping leads necessarily to a number of breakthrough points equal to the number of injection points since coalescence of flow paths is not possible. This is, however, wrong (when the number of active bonds at the inlet is sufficiently large, of course). In fact, a pore adjacent to an inlet active bond can be occupied by the invading phase as a result of a previous invasion. As a result, there is no creation of a new flow path when this bond is activated. Thus, the number of breakthrough points is lower than the number of active bonds (or equal, at most, when there is a limited number of active bonds at the inlet). This is illustrated in Fig. 3(d) with only two breakthrough points originating from 15 inlet active bonds.

Differences between the sequential algorithm and the kinetic algorithm due to trapping are also expected with partial trapping. This is illustrated in Fig. 3. One important consequence of trapping is that injection bonds at the inlet become inactive as the result of trapping. This occurs when a defending phase cluster in contact with the inlet becomes trapped as a result of invading fluid invasion. When this happens, it is assumed that all the inlet bonds connected to this cluster cannot be active since invasion is not allowed in a trapped cluster. With the kinetic algorithm, all active bonds at the inlet are activated simultaneously. Consider the sequential algorithm and suppose that the first two flow paths generated coalesce and form a trapped cluster in contact with the inlet. All bonds in contact with this cluster cannot be activated. With the kinetic algorithm the zone corresponding to this trapped cluster is invaded at least partially since there is invasion from the inlet bonds in contact with this zone as long as this zone is not trapped. This is illustrated in Figs. 3(b) and 3(c) which show trapping along the inlet with the sequential algorithm but not with the kinetic algorithm.

Also, it can be anticipated that the kinetic algorithm leads to more breakthrough points compared to the sequential algorithm when trapping is perfect. This illustrated in Figs. 3(d) and 3(e). The number of breakthrough points is 2 with the sequential algorithm and 3 with the kinetic algorithm. This is essentially due to the fact that more single trapped bonds are trapped with the kinetic algorithm (a single trapped bond is a bond of defending phase trapped between two pores occupied by the invading phase; see Fig. 3). Consider two first neighbor pores in the first row of pores connected to inlet bonds. These two pores cannot belong to the same flow path with the kinetic algorithm with perfect trapping because the bond in the first row connecting them is automatically trapped as a result of the simultaneous invasion of the two pores. With the sequential algorithm, the invasion of the two pores is not simultaneous. On the contrary, the invasion of the second pore to be invaded only occurs when the first pore has been fully invaded. As a result the second pore can be invaded from the first pore and therefore can belong to the same flow path as the first pore, which is impossible with the kinetic algorithm.

E. Mixed wettability

As mentioned in the Introduction, a porous system of mixed wettability is a system in which some regions are hydrophilic (or more generally wetting for the invading phase) and others hydrophobic (nonwetting for the invading phase). The spatial distribution of hydrophilic and hydrophobic regions is often not well known and can also change with time. It is therefore interesting to study what happens when the fraction of hydrophilic regions is varied. The simple model used in the present article is to consider that a fraction f of the pores and the throats in the network is hydrophilic, the hydrophilic pores and throats being selected randomly. In other terms, f is the probability of a pore (and a throat) being hydrophilic in the network. No correlation between the hydrophilicity of a pore and adjacent throats is introduced. Hydrophilic pores and hydrophilic bonds are randomly selected independently. The distinguishing features introduced by the consideration of hydrophilic elements (pores or throats) is that the invasion potential of pores and throats depends on the local wettability property and in the case of a pore of the local distribution of the fluids in neighbor throats [3,8].

The invasion potential of a bond can be defined as before as $\phi = -2a\cos\theta/w_b$, where θ is the contact angle ($\theta < 90^\circ$ in a hydrophilic element and $\theta > 90^\circ$ in a hydrophobic element). Similarly, the invasion potential of a hydrophobic pore can be defined as $\phi = -2a\cos\theta/w_p$. As mentioned before, the invasion potential of a hydrophilic pore depends on the number

of adjacent throats already invaded. A simple expression adapted from [9] reads

$$\varphi = -2a\cos\theta\,[1 + 0.25\,(m-1)]\,/w_p, \qquad (1)$$

where m is the number of adjacent throats already occupied by the invading fluid. This expression is consistent with experimental observations which show that the probability of invasion of a pore decreases with the number of throats containing the nonwetting phase connected to it. The interested reader can refer to [8–10] for more details. In what follows, we have taken $\theta = 110^\circ$ in hydrophobic regions and $\theta = 80^\circ$ in hydrophilic regions. These values are representative of GDL (see Sec. V) but what matters here is to impose a relevant hierarchy in the invasion potential [8]. The results are in fact not sensitive to the particular values of θ chosen, respectively, for the hydrophilic and hydrophobic regions as long as $\theta < 90^\circ$ in hydrophilic regions and $\theta > 90^\circ$ in hydrophobic regions.

III. INFLUENCE OF TRAPPING PHENOMENA

A. Breakthrough point statistics

In this section, we study the statistics of breakthrough points at the end of displacement for $n_i = 100\%$. Figure 4 shows the evolution of $\langle N_{\rm BT}\rangle / N_x^2$, i.e., the probability that an outlet bond is a breakthrough point, as a function of thickness N_z [the brackets $\langle\cdots\rangle$ mean the (ensemble) average over numerous ($= 500$) realizations for two lateral network sizes ($N_x = N_y = 20$ and $N_x = N_y = 40$]. As can be seen the average number of breakthrough points is always significantly lower that the number of active injection bonds at the inlet.

We know from the results presented in [1] that the probability $\langle N_{\rm BT}\rangle / N_x^2$ depends only on N_z for a sufficiently thin system; i.e., it does not depend on the lateral size N_x of the system (see [1] for more details). This was for hydrophobic systems in the absence of trapping. As shown in Fig. 4, this still holds when trapping is taken into account. As indicated in the caption of Fig. 4, the results are identical between the simulations without trapping and with partial trapping. Consistently with the results presented in [1], the sequential and kinetic algorithms lead to the same result in this case. As shown in Fig. 3 [compare Figs. 3(a)–3(c)], this is not the case in two dimensions except when the system is extremely thin ($N_z \leqslant 4$ to 5), [11]. For thicker 2D systems, the number of breakthrough points increases when trapping is taken into account and the results are different depending on the used algorithms, sequential or kinetic. As can be seen from Fig. 4, the situation is different when perfect trapping is considered. This is in accordance with the considerations of Sec. II D. As for the case without trapping, e.g., [1], four regions can be distinguished in the evolutions shown in Fig. 4 depending on the thickness of the system, namely the ultrathin system region, the power law region, the thick system region—the third region being the intermediate region between the power law region and the thick system region. The power law region is observed when the system is not too thin and is well described

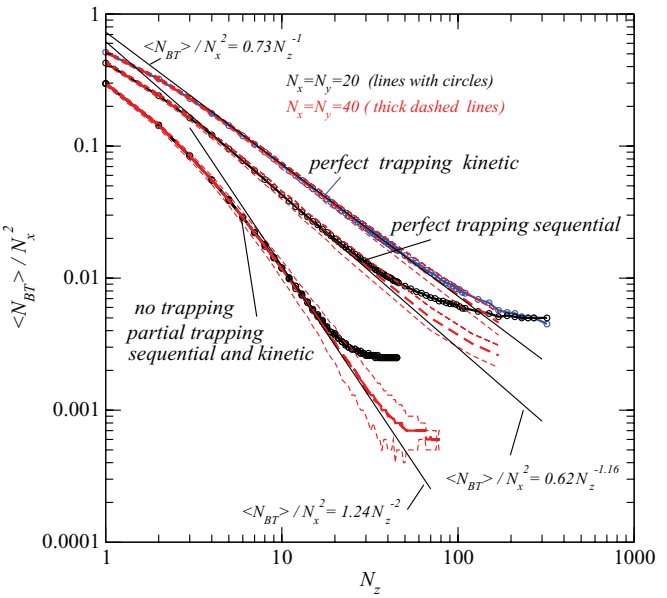

FIG. 4. (Color online) Influence of trapping and flow scenario on the probability that an outlet bond is a breakthrough point when all inlet bonds are active at the inlet ($n_i = 100\%$). The thin dashed curves for $N_x = 40$ represent ± 1 standard deviation around the mean value. For each curve, four regions are distinguished depending on the thickness N_z of the system: (1) the ultrathin system region when the system is very thin, (2) the power law region for larger thicknesses right after the region of ultrathin systems, (3) a transition region between the power law region and region 4, (4) the thick systems characterized by only one or two breakthrough points (plateaus on the right-hand side in the figure, noticing that only the beginning of plateaus is shown). The extent of the ultrathin system region, the exponent of the power law region and the number of breakthrough points when the system is thick depend on the flow and trapping scenarios. Note that the results of the simulations without trapping and with partial trapping are identical.

by a power law relationship of the form

$$\frac{\langle N_{\rm BT}\rangle}{N_x^2} \approx \lambda\, N_z^{-\alpha}. \qquad (2)$$

The exponent α is equal to 2 in the absence of trapping [1]. As can be seen from Fig. 4, the exponent is still 2 with partial trapping but becomes significantly smaller ($\alpha = 1$ for the kinetic invasion, $\alpha \approx 1.16$ for the sequential invasion) when perfect trapping is considered. The numeral prefactor remains of $O(1)$ for all cases considered. Thus, the number of breakthrough points for a given thickness is greater when perfect trapping is considered and the greatest with the kinetic invasion. This also holds for the ultrathin systems, which are defined as the systems whose thickness is smaller than the thickness marking the beginning of the power law behavior. The variation of $\langle N_{\rm BT}\rangle / N_x^{21}$ is slower than the one given by Eq. (1). The thickness marking the transition between the ultrathin system behavior and the power law behavior is lower when perfect trapping is considered ($N_z = 3{,}4$ with perfect trapping, $N_z \approx 10, 15$ in the absence of trapping or with partial trapping). As discussed in Sec. II D, the effect of trapping is to reduce the number of active bonds (initially active inlet bonds become inactive when connected to a trapped cluster)

and to reduce the flow path coalescence. It is expected that the first effect leads to a decrease in the number of breakthrough points (less inlet active bonds) whereas the second effect tends to increase the number of breakthrough points (less coalescence). As can be seen from Fig. 4, the coalescence phenomenon is quite frequent in the absence of trapping since the number of breakthrough points is always much smaller than the number of injection points. Thus a sufficiently thin system is flow path coalescence sensitive. As a result, any phenomenon reducing the coalescence probability has a significant effect. This explains why more breakthrough points are obtained when perfect trapping is considered. The reasons explaining the greater probability for an outlet bond to be a breakthrough point when invasion with perfect trapping is kinetic compared to sequential are given in Sec. II D and are therefore not repeated here.

Interestingly also, the average number of breakthrough points in a sufficiently thick system (right-hand side plateau in Fig. 3) is 2 in our simulations when trapping is perfect whereas the number of breakthrough points is 1 in the absence of trapping or when trapping is partial. This corresponds to the fourth region (thick systems). Whereas a single breakthrough point is always expected for a sufficiently thick system in the absence of trapping or when trapping is partial, it is actually expected that the number of breakthrough points for a thick system when trapping is perfect depends on the lateral size N_x of the network.

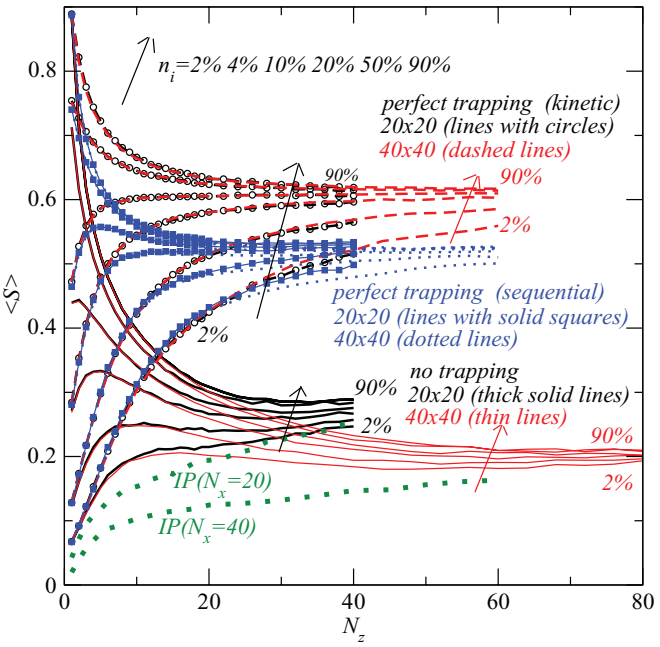

FIG. 5. (Color online) Invading phase mean overall saturation as functions of porous layer thickness and fraction of active injection inlet bonds n_i for various flow and trapping scenarios. The curves labeled IP (invasion percolation) are obtained using the standard invasion percolation algorithm with the traditional boundary condition (see text).

B. Saturation

In addition to the statistics of breakthrough points, an important aspect in this problem concerns the fluid distribution within the system. The pore space fluid occupancy is characterized by the invading fluid overall saturation S (=volume fraction of the pore space occupied by the invading phase) at the end of displacement. Partial trapping leads to the same results as in the absence of trapping in three-dimensional (3D) systems whatever the algorithm used, consistent with the results obtained for the number of breakthrough points discussed in the previous section. It is difficult to form large trapped clusters in 3D when trapping is partial. The results are again quite different when trapping is considered as perfect. As can be seen from Fig. 5, the overall saturation at the end of displacement is significantly greater than in the absence of trapping and the kinetic algorithm leads to greater saturations than the simpler sequential algorithm. Since the mechanism of coalescence by invasion of a bond is not possible in perfect trapping, the net result is that the invading phase, which is formed by a series of independent flow paths, is forced to visit regions that would not be visited otherwise (i.e., when trapping is partial or in the absence of trapping). As noted in Sec. II D before, the sequential algorithm leads to more trapping of the defending phase. This explains why the saturation is lower with the sequential algorithm compared to the kinetic algorithm when trapping is perfect.

There is a significant lateral scale dependence in the absence of trapping (or when trapping is partial) except, interestingly, when the system is sufficiently thin. This was already noticed in [1], where it is shown that the percolation scaling $\langle S\rangle \propto g(\frac{N_z}{N_x},n_i)N_x^{-0.48}$ applies to describe this scale dependence (function g is shown in Fig. 12 in [1]). When trapping is perfect, the bond or pore occupation probability by the invading phase is much greater (as shown in Fig. 5), thus far from the network percolation threshold (see [1] for more details), and the lateral scale dependence disappears (except when the fraction of inlet active injection bonds is very low). This introduces a major difference between perfect trapping and no trapping or partial trapping, since when the trapping is perfect $\langle S\rangle$ depends only on system thickness N_z and n_i but not anymore on lateral size N_x (except again when n_i is very small and the invasion sequential). Also, it can be seen from Fig. 5 that the traditional IP algorithm significantly underpredicts the saturation. The traditional IP algorithm means the IP algorithm with the traditional free fluid layer boundary condition at the inlet [2] (as briefly described in the Introduction).

C. Defending phase transport capacity (diffusion conductivity)

The defending phase access to the inlet can be a crucial aspect in some applications. For example, a defending phase percolating cluster between the outlet and the inlet should exist for the system discussed in Sec. V to work. This is clearly not possible when all inlet bonds are injection bonds ($n_i = N_i/N_x^2 = 1$) since a defending phase percolating cluster cannot exist in this case. This becomes possible when the fraction of active inlet injection bonds is diminished, at least when the system is sufficiently thin.

The defending phase transport capacity can be characterized considering the diffusive transport of a species through the defending phase percolating subnetwork. In the porous

medium literature, e.g., [12], the effect of the porous structure on the binary diffusion process in the pore space is usually analyzed through the consideration of the effective diffusion coefficient D^* of the porous medium, which becomes a function of the saturation (e.g., see [13]) when a fraction of the pore space is partially blocked by another fluid. This is a useful concept in the context of the continuum approach to porous media, that is, when the usual conditions of length scale separation are met, e.g., [14]. The situation is different here because of the lack of length scale separation between the porous layer thickness and the pore size. In this case, it is more appropriate to consider the apparent diffusion overall conductivity G_D of the whole layer, which is defined by

$$J = AG_D\Delta C, \tag{3}$$

where J is the diffusive mass rate through the porous layer when a concentration difference ΔC is applied across the porous layer, $A = L \times L$ is the cross-section area of the porous layer. Thus, we impose the concentration C_0 in the first plane of pores occupied by the defending phase at the inlet, and the concentration $C_0 - \Delta C$ in each pore occupied by the defending pore at the outlet. J is computed from the solution of the diffusion problem over the defending phase under steady-state condition. The method of solution is described in many previous works and is therefore not described in detail here again, e.g., Refs. [15,16], and references therein. The problem is in fact fully analogous to a random electrical resistance network problem. Choosing D/a as a reference conductance, where D is the binary diffusion coefficient in the free fluid and a the lattice spacing, we consider in the following the dimensionless overall conductance $G_D^* = \frac{G_D}{(D/a)}$.

Figure 6(a) shows the variation of G_D^* as a function of the system thickness for various fractions of active injection bonds at the inlet when trapping is neglected. Interestingly, the conductance decreases significantly with the layer thickness in the range of ultrathin systems ($N_z < 10{,}15$) whereas the variation with the thickness is quite slow when the system is thicker. This figure again shows that there is no lateral scale dependence when the system is sufficiently thin.

As can be seen from Fig. 6(b), the perfect trapping has a spectacularly detrimental impact on G_D^*. This is of course consistent with the impact of perfect trapping on pore occupancy by the invading phase which is much greater for the same condition compared to the case where trapping is partial or negligible (see Fig. 5). Also, it can be noted that the difference on G_D^* between the kinetic and sequential algorithms with perfect trapping is relatively weak (less than for the saturation; see Fig. 5) when the system is well connected (defending phase far from percolation threshold). The difference is much more marked when the defending phase approaches the percolation threshold [range of values of G_D^* below about 0.001 in Fig. 6(b)]. Note also that the sequential algorithm with perfect trapping leads to lower values than the kinetic algorithm with perfect trapping when n_i is sufficiently small [$n_i = 2\%$ in Fig. 6(b)], whereas the opposite is found for greater values of n_i. This is consistent with the impact of n_i on the defending phase percolating cluster saturation (not shown) which indicates that the kinetic algorithm leads to a greater saturation for low values of n_i and to a lower saturation

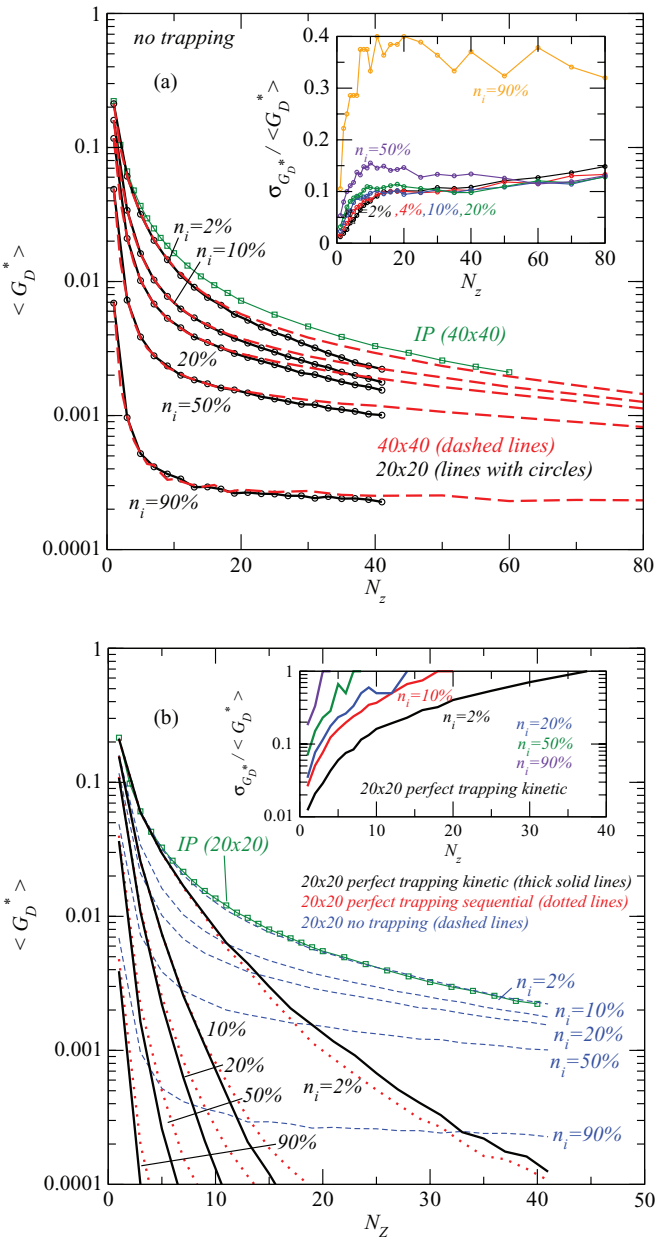

FIG. 6. (Color online) (a) Variation of defending phase diffusive dimensionless conductance G_D^* as a function of system thickness for various fractions of active injection bonds at the inlet when trapping is neglected. The curves labeled IP (invasion percolation) are obtained when the standard invasion percolation algorithm with the traditional boundary condition is used to compute the fluid distribution. The inset shows the variation of the reduced standard deviations as a function of system thickness for networks of size $40 \times 40 \times N_z$. (b) Variation of defending phase diffusive conductance G_D^* as a function of the system thickness for various fractions of active injection bonds at the inlet for different trapping and flow scenarios. The inset shows the variation of the reduced standard deviations as a function of system thickness for the perfect trapping scenario using the kinetics algorithm.

for sufficiently large values of n_i compared to the sequential algorithm. In the remainder of this section, we further discuss the case without trapping, which is *a priori* more representative of the porous systems motivating the study (see Sec. V).

The results obtained using the standard invasion percolation algorithm (no trapping, classical boundary condition) are shown in Fig. 6(a) [curve labeled IP in Fig. 6(a)]. As can be seen, using the standard IP algorithm leads one to significantly overestimate the conductance. The conductance obtained using the standard IP algorithm is comparable with the one obtained with the multiple injection boundary condition (BC) only when the fraction of active injection bonds at the inlet in the multiple injection scenario is quite low, on the order of 1–2%. Thus the multiple injection BC has a quite significant impact on the results.

Despite the lack of length scale separation, the traditional continuum (mean field) approach, e.g., [17], is used very frequently in the literature. As a result the diffusive rate through the layer is expressed as

$$J = AD^* \frac{\Delta C}{W}, \tag{4}$$

where W is the layer thickness [$W = (N_z - 1)a$]. Then it is generally assumed that the sole consideration of the overall saturation is sufficient to take into account the impact of pore occupancy by the nonconducting phase on transport. Accordingly, the effective diffusion coefficient D^* is expressed as a function of the overall saturation only. A very often used expression, referred to as the Bruggeman relationship, e.g., [16,18], is given by

$$D^*(S)/D = \varepsilon^{1.5}(1 - S)^{1.5}, \tag{5}$$

where S is the nonconducting phase saturation. Notice that $G_D^* = \frac{1}{N_z}\frac{D^*}{D}$.

Our results clearly indicate that this type of approach is not correct when the system is thin and there are multiple injections at the inlet. This is illustrated in Fig. 7. To construct Fig. 7 we have computed $D^*(N_z,n_i)/D$ and $S(N_z,n_i)$ varying N_z in the range [1, 40] and n_i in the range [0.02, 0.9] and then plotted $D^*(N_z,n_i)/D$ as a function of S (N_z,n_i). As can be seen from Fig. 7, the apparent diffusion coefficient in our case (multiple injection) is not only a function of $\langle S \rangle$ but also of system thickness, thus scale dependent, at least for the sufficiently thin systems which are of primary interest for the present study. By contrast, the reduced apparent coefficient depends only on S in a sufficiently thick system. It can be also noted that Eq. (5) is not adapted to describe our results.

In brief, in disagreement with many previous works, our results show that the traditional continuum concepts lead here to very poor approximations of the transport because of the lack of length scale separation characteristic of thin systems and because of the phase distribution associated with the considered quasistatic invasion regime. As a result, the "effective" (apparent in fact) diffusion coefficient is thickness dependent (as for a traditional IP process; see Fig. 7) and also varies with the number of active inlet injection bonds. For a given thickness, our results indicate, however, that the apparent diffusive coefficient, or better the diffusive conductance, is a decreasing monotonic function of the overall saturation. The functional form of this function depends on the thickness as shown in Fig. 7.

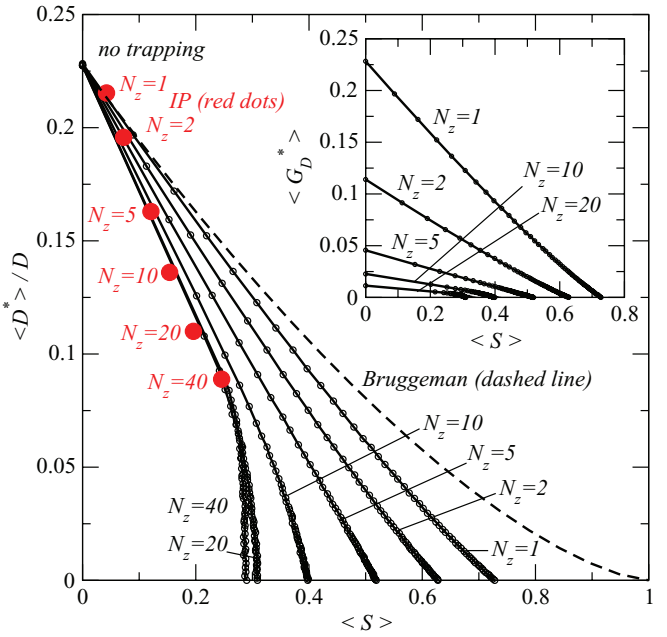

FIG. 7. (Color online) Variation of defending phase apparent diffusion coefficient as a function of saturation for different system thicknesses. The big solid circles are the results obtained when the standard invasion percolation algorithm with the traditional boundary condition is used to compute the fluid distribution. The inset shows the variation of defending phase diffusive conductance G_D^* as a function of saturation for different system thicknesses.

D. Statistical fluctuations

Another characteristic of thin systems is that statistical fluctuations from one sample to another can be significant, at least when the lateral extension N_x is not too large compared to the thickness N_z. This is illustrated in Fig. 8, which shows

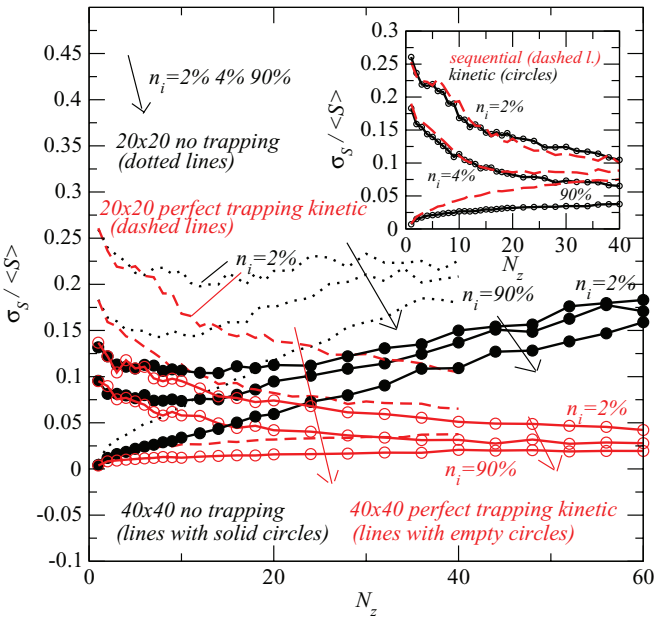

FIG. 8. (Color online) Variation of reduced standard deviation of the invading phase saturation for no trapping and perfect trapping and the two flow scenarios.

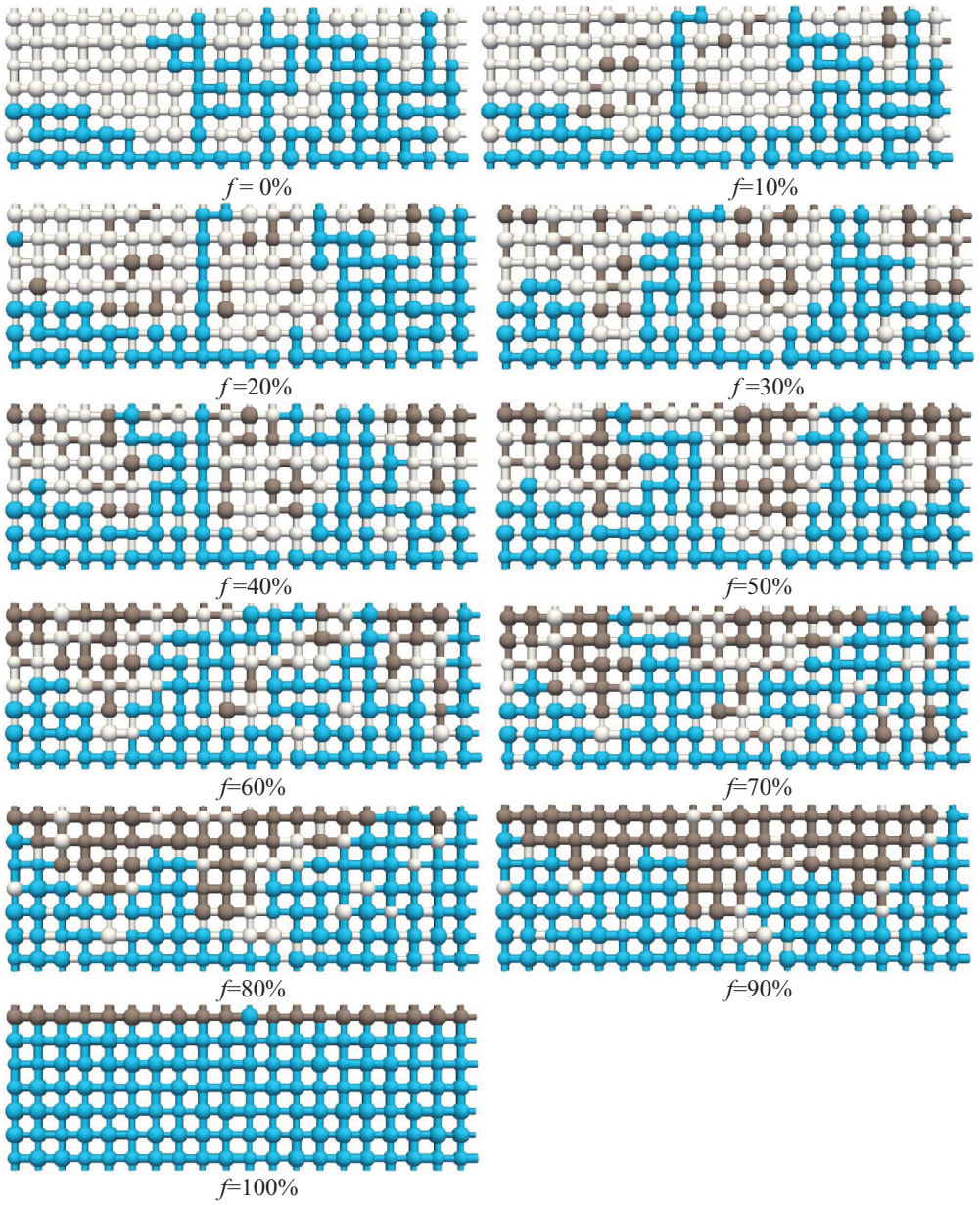

FIG. 9. (Color online) Invasion patterns in a small two-dimensional network for various fractions of hydrophilic pores in the absence of trapping when all inlet bonds are active. Invading fluid in light gray (blue online), defending fluid in white (in hydrophobic pores and bonds) or dark (in hydrophilic pores or bonds). The breakthrough points correspond to the outlet bonds in light gray (blue online).

the standard deviation of the invading phase saturation over the realizations considered. The reduced standard deviation $\sigma_s/\langle S\rangle$ is typically on the order of 01–0.2 when the system is thin.

As shown in Fig. 8, perfect trapping has a significant impact on the saturation fluctuation from one realization to the other. Consistently with the fact that the saturation is greater (and therefore the structure of the invading phase more compact since the bond occupation probability is far from the percolation threshold), the saturation statistical fluctuations are significantly lower when trapping is perfect, and the lowest for a given size with the kinetic invasion, consistently with the fact that the kinetic invasion with perfect trapping leads to the greatest saturation (see inset in Fig. 8). Contrary to the average overall saturation, which does not depend (or only weakly for the small values of n_i) on the lateral size N_x, the effect of N_x on the standard deviation of S is noticeable and can be attributed to finite size effects ($\sigma_S/\langle S\rangle$ decreases with N_x for a given N_z). Hence, when $N_x \gg N_z$ the statistical fluctuations of S are expected to die out.

The evolution of the standard deviation of G_D^* is shown in the inset of Fig. 6(a) when trapping is neglected and in the inset of Fig. 6(b) when trapping is perfect. As can be seen the fluctuations can be quite significant when the invading phase saturation is high (high values of n_i), that is, when the percolating defending (conducting) phase tends to form a poorly connected cluster.

IV. MIXED WETTABILITY

The impact of mixed wettability is studied in this section. Except for the patterns shown in Sec. IV A, we consider 3D systems and neglect trapping phenomena. According to the previous section (Sec. III), the results should be representative of partial trapping as well but we have not checked, in fact, if the results are still identical between no trapping and partial trapping when the wettability is mixed. The fact that the invasion pattern becomes increasingly compact as the fraction f of hydrophilic elements increases (see Sec. IV A) suggests, however, that this is probably the case.

The main parameters are the lateral size of the system N_x (we recall that $N_y = N_x$ throughout the paper), its thickness N_z, the fraction n_i of active injection bonds at the inlet, and the fraction f of hydrophilic elements. The study of the influence of these parameters is organized as follows. After a brief discussion on the influence of f on the invasion patterns, we study the influence of f, N_x, and N_z on the number of breakthrough points for $n_i = 100\%$ in Sec. IV B. The influence of f on the pore occupancy by the defending phase and the diffusive conductance varying N_x and N_z is studied in Secs. IV C and IV D, respectively, for a fixed n_i ($n_i = 10\%$). Then we end this part of the paper looking in Sec. IV F at the influence of both n_i and f for a given thickness selected in the range corresponding to thin systems ($N_z = 10$).

A. Invasion patterns

It is well known from previous studies, e.g., [3,8], that the invasion pattern in the quasistatic limit is compact in a uniformly hydrophilic system whereas the pattern is ramified and characterized by capillary fingering in a hydrophobic system. Thus, even with the multiple injection boundary condition, we expect that the pattern changes from ramified (IP pattern) to compact as f increases in the range [0,1]. This is illustrated in Fig. 9 for a small 2D network. This is due to cooperative mechanisms between adjacent menisci in pores.

The invading phase favors the hydrophilic elements and tends to avoid the hydrophobic ones. As a result, the invading phase invades only the hydrophilic element when there exists a percolating path of hydrophilic elements between a given injection bond at the inlet and the outlet.

With the traditional boundary condition (porous layer in contact with an invading phase reservoir at the inlet), this leads to the introduction of the percolation threshold f_c of the hydrophilic network; see [19]. This is illustrated in Fig. 10, which also shows that f_c (defined simply here as the value corresponding to the percolation probability of 0.5) increases with the system thickness (see top inset in Fig. 10). Hence when $f > f_c$ the probability that the hydrophilic elements form a percolating cluster is large (as shown in Fig. 10, the percolation transition is not sharp because of finite size effects), and the invading phase has therefore a great probability to take a path of hydrophilic elements between the inlet and the outlet. As shown and discussed in [19], the invasion patterns are quite similar, i.e., ramified, when $0 \leqslant f \leqslant f_c$. As result, the pore occupancy (saturation) and the transport properties (diffusive conductance, for example) depend only weakly on f when f is in the range $0 \leqslant f \leqslant f_c$. By contrast,

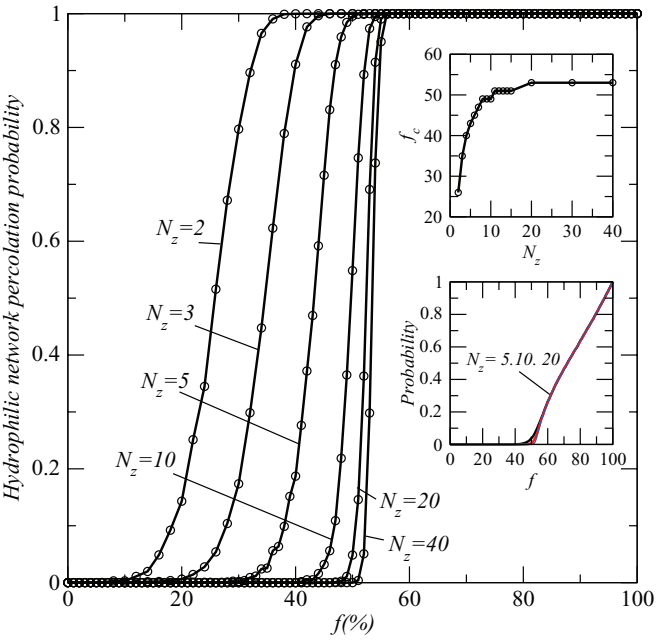

FIG. 10. (Color online) Variation of hydrophilic (sub-) network percolation probability as a function of the fraction f of hydrophilic elements in the network for various network thicknesses. The top inset shows the influence of system thickness on percolation threshold (see text). The bottom inset obtained for $n_i = 10\%$ shows the evolution of the probability that an active injection point belongs to a hydrophilic percolating cluster.

all properties vary significantly with f when $f_c \leqslant f \leqslant 1$; see [19] for more details. This is for the traditional boundary condition. With the multiple injection boundary condition, we expect a situation somewhat similar but more complicated since the invasion is solely through hydrophilic elements only when all injection bonds are connected to hydrophilic element percolating clusters. Also, for a given layer thickness and a given lateral extension, we can concentrate only on the impact of f with the traditional boundary condition. Here we have the additional parameter n_i. We have not attempted a comprehensive study of the percolation probability of the hydrophilic network varying n_i and N_z. We only discuss briefly the results shown in the bottom inset in Fig. 10 obtained with $n_i = 10\%$. This inset shows the evolution of the probability that an active injection point belongs to a hydrophilic percolating cluster. In contrast with the classical boundary condition, the invasion is not through hydrophilic elements only when $f_c \leqslant f < 1$. However, as shown in the bottom inset in Fig. 10, the probability for an active injection point to belong to a hydrophilic percolating cluster increases quite rapidly with f above f_c. As a result, we expect here also a quite significant influence of f on the phase distribution and the transport properties when f is greater than f_c.

B. Breakthrough point statistics

The influence of mixed wettability on the average number of breakthrough points is discussed in this section varying f and N_z (for $n_i = 100\%$). As can be seen from Fig. 11, two regions can be distinguished as expected: a first region, where the probability $\langle N_{\mathrm{BT}} \rangle / N_x^2$ that an outlet bond is a breakthrough

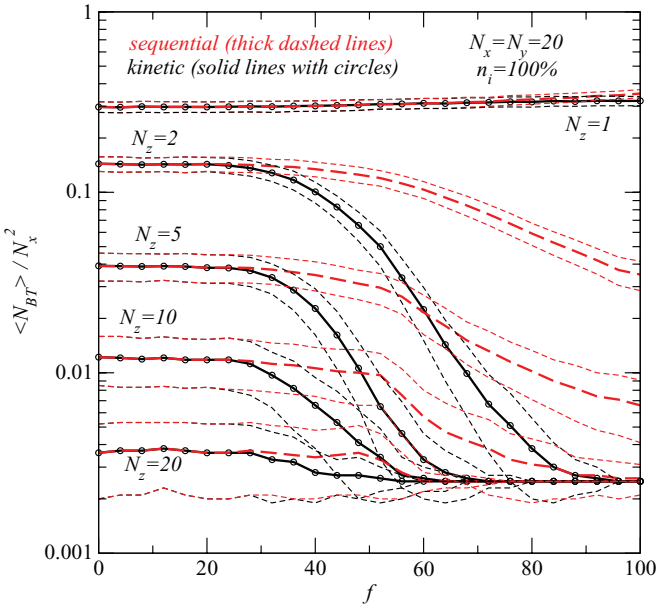

FIG. 11. (Color online) Probability that an outlet bond is a breakthrough point as a function of the fraction of hydrophilic elements for various network thicknesses N_z when all inlet bonds are active at the inlet ($n_i = 100\%$). The dashed curves represent ± 1 standard deviation around the mean value.

bond does not depend on f (roughly for $0 \leqslant f \leqslant 30\%$ with the kinetic algorithm and for $0 \leqslant f \leqslant 40\% - 50\%$ with the sequential algorithm), then a region where the influence of the fraction f of hydrophilic elements is quite significant (for a sufficiently thin system if one discards the quite particular case $N_z = 1$ and especially with the kinetic algorithm). $\langle N_{\mathrm{BT}}\rangle / N_x^2$ decreases with f in the second region, which is consistent with the fact that the invasion pattern is less and less ramified and thus more and more compact as f increases in this range of f (Fig. 9). Interestingly, the impact of f on the number of breakthrough points is particularly marked when the system is very thin ($N_z \leqslant 10$).

The differences observed between the sequential and kinetic algorithms can be explained as follows. Consider a hydrophilic pore. It is possible with the kinetic algorithm that this pore is reached by two independent flow paths at (about) the same time. As a result, its invasion potential increases since the invasion potential of a pore increases with the number of adjacent bonds filled with the invading fluid (see Sec. II E). Denote by ϕ_1 this invasion potential. With the sequential algorithm, this pore is reached by only one flow path. It is therefore likely that the invasion potential of the pore in this case, denoted by ϕ_2, is lower than ϕ_1. It is also quite likely that there exists an element of invasion potential ϕ along the invading phase – defending phase interface such that $\phi_2 \leqslant \phi \leqslant \phi_1$. As a result, the invasion pattern is different depending on the used algorithm. This reasoning indicates also that the pattern has a greater probability to be more compact with the kinetic algorithm since the cooperative growth of menisci in pores is more likely. This is consistent with the much marked effect of f on $\langle N_{\mathrm{BT}}\rangle / N_x^2$ with the kinetic algorithm for $f \geqslant 25\%$ shown in Fig. 11.

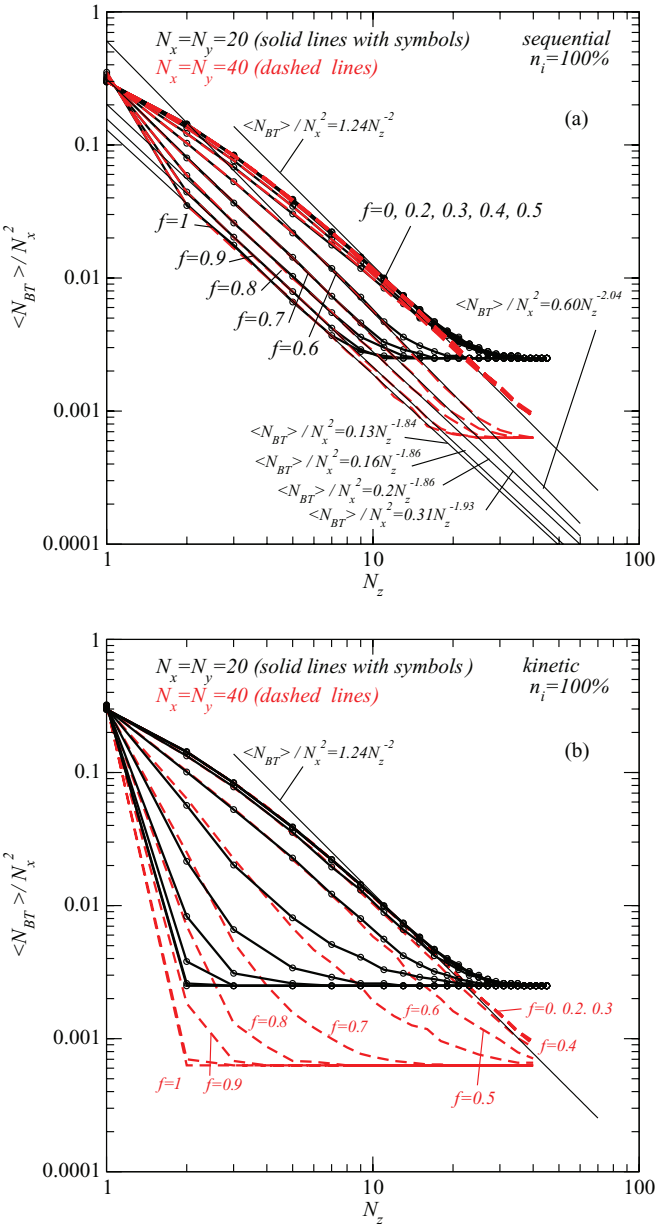

FIG. 12. (Color online) Probability that an outlet bond is a breakthrough point when all inlet bonds are active at the inlet ($n_i = 100\%$) as a function of system size for various fractions of hydrophilic elements: (a) sequential flow scenario, (b) kinetic flow scenario.

The influence of f is further illustrated in Fig. 12. Again, one can clearly distinguish a range of f below a certain value (50% with the sequential algorithm, 30% with the kinetic algorithm) in which there is a very weak influence of f on $\langle N_{\mathrm{BT}}\rangle / N_x^2$. For greater values of f, the influence is marked and the effect of increasing the fraction of hydrophilic elements is to reduce the number of breakthrough points.

It can be also observed in Fig. 12(a) that several breakthrough points are still possible with a purely hydrophilic system ($f = 100\%$) with the sequential algorithm, i.e., more generally when the injections are not activated simultaneously but at sufficiently different times, when the system is very thin [$N_z < 10$ in Fig. 12(a)]. Hence several invading phase

percolating clusters can be formed when the injection is sequential (the condition is of course that some of the activated inlet bonds are selected sufficiently far away from the inlet bonds previously activated in the sequence). This is in complete contrast with the results for the kinetic algorithm depicted in Fig. 12(b), which show that only one breakthrough point forms when $f = 100\%$ whatever the thickness of the network (if again we discard the very particular case $N_z = 1$). Note, however that the invasion is fully compact in this case (see Fig. 9), which means that there are invading phase menisci right beneath every outlet bond (aside from the one corresponding to the breakthrough point). Also, it can be noted that here we must not see a droplet of the invading phase forming at the exit of the breakthrough bond, which is the situation expected when the porous medium is hydrophobic, but most probably the development of a wetting film all over the porous medium surface from the breakthrough bond exit. The coalescence of the film with the menisci previously mentioned is likely to lead to a full flooding of the porous layer.

As for the cases discussed in Sect. III, one observes a region in the curves shown in Fig. 12(a) which can be described by a power law. As can be seen from Fig. 12(a), the exponent of the power law decreases as f increases above f_c. Also, if one discards the particular case corresponding to $N_z = 1$, it can be seen that the power law relationship describes the full range of data (up to the probability $1/N_x^2$, of course) when f is sufficiently large above f_c [$f \geqslant 0.7$ in Fig. 12(a)]. This is contrast with the case of the sequential invasion in a hydrophobic system (or partially hydrophobic system as long as $f < 0.7$), which cannot be described by a power law behavior in the range of thin systems ($N_z \leqslant 10$).

It can be also noticed again that the results do not depend on the lateral size of the system when the system is sufficiently thin [except as shown in Fig. 12(b) with the kinetic algorithm and f sufficiently close to 1].

The results are different when the invasion is kinetic. As can be seen from Fig. 12(b), the power law behavior is not obtained anymore when $f > 0.5$.

C. Saturation

In the same spirit as in Sec. III, the influence of f on the pore occupancy is discussed in this section. Throughout this subsection and the next one we consider only the case $n_i = 10\%$ (so as to have a reasonably large probability that the defending phase can form percolating clusters). Also we consider only one lateral size, namely $N_x = 20$. We believe that the influence of lateral size can be, at least qualitatively, inferred from the results presented in Sec. III. We begin with the evolution of the invading phase overall saturation, which is shown in Fig. 13(a). One can distinguish two main regions, below and above the percolation threshold f_c of the hydrophilic subnetwork. According to Fig. 10, $f_c \sim 0.5\%$ whereas the value marking the transition between the two regions is shifted to the right in Fig. 13(a), $f_c \sim 0.65$ to 0.7. This is an effect of the discrete injection (see bottom inset in Fig. 10). As can be seen from Fig. 13(b), the results obtained with the traditional boundary condition do not shown such a shift. For convenience, f_c also denotes the shifted value in what follows.

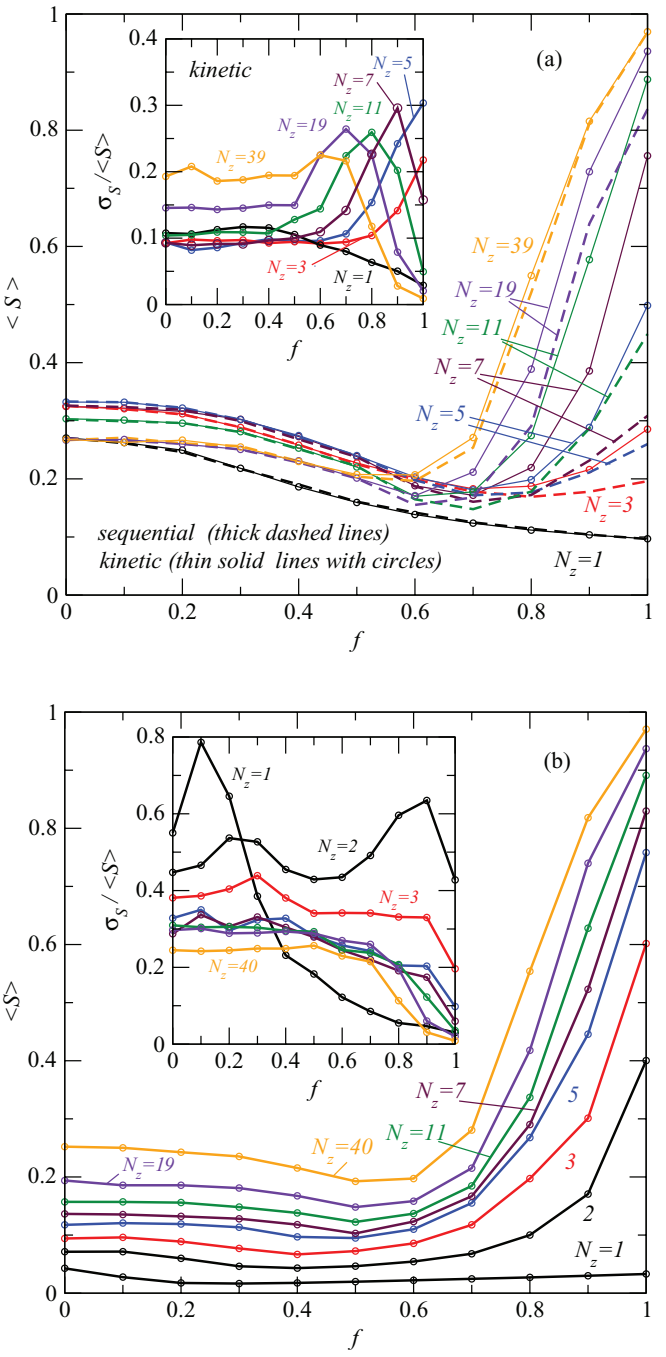

FIG. 13. (Color online) Variation of invading phase saturation as a function of the fraction of hydrophilic elements in the network for various system thicknesses (computed on $20 \times 20 \times N_z$ networks with $n_i = 10\%$): (a) sequential and kinetic flow scenarios, (b) traditional boundary condition (see text). The insets show the reduced standard deviation of S.

Both Fig. 13(a) (discrete injection) and Fig. 13(b) (traditional boundary condition) show that the influence of f is much less marked for $f < f_c$ compared to the region $f > f_c$. The saturation increases quite significantly when f varies in the range $[f_c, 1]$ except when the system is extremely thin [$N_z \leqslant 3$ in Fig. 13(a), $N_z < 2$ in Fig. 13(b)]. The kinetic and sequential algorithms lead to the same results when $f < f_c$ whereas a greater saturation is obtained with the kinetic algorithm when

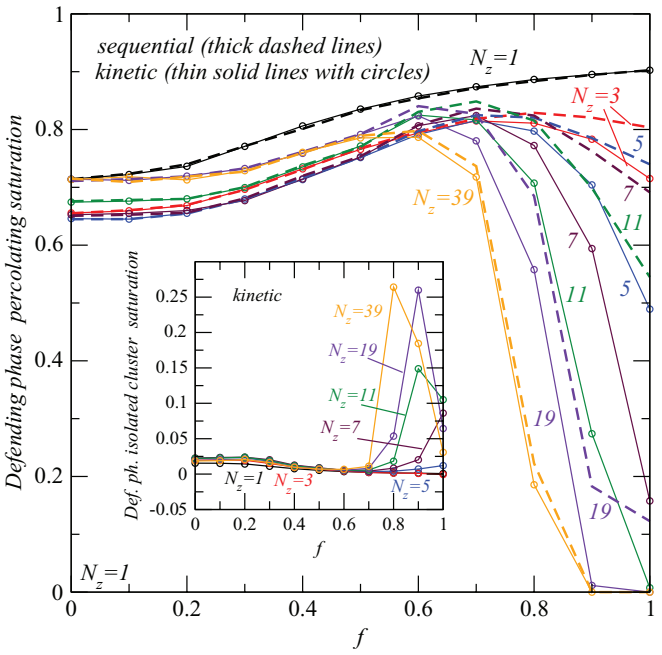

FIG. 14. (Color online) Variation of defending phase saturation as a function of the fraction of hydrophilic elements in the network for various system thicknesses (computed on $20 \times 20 \times N_z$ networks with $n_i = 10\%$). The main figure shows the saturation corresponding to the percolating clusters of the defending phase whereas the inset shows the saturation corresponding to the isolated (nonpercolating) clusters.

$f > f_c$ [Fig. 13(a)]. Also, we note that the traditional boundary conditions leads to lower saturation when $f < f_c$ compared to the discrete injection whereas the opposite can be observed when $f > f_c$.

We now discuss the percolating properties of the defending phase through the computation of $S_{dppc}(N_x, N_z, f)$, that is the volume fraction of the pore space occupied by the defending phase belonging to percolating clusters. As can be seen from Fig. 14, one can again distinguish two main regions as regards the influence of f. In the range [0–70%], the saturation S_{dppc} remains high, above 0.65, and varies relatively little with the system thickness. As before, there is a subrange, $0 \leqslant f \leqslant 20\%$, in which the value of f has a negligible influence. Interestingly, the saturation increases with f in the range [20–60%], which could appear as somewhat counterintuitive. A naïve view is to consider that increasing the fraction of hydrophilic elements favors compact invasion patterns and therefore should decrease the defending phase saturation. The saturation increases with f is much more marked in the subrange [40–60%], which corresponds to the range of f where entirely hydrophilic percolating paths form according to the results shown in the bottom inset in Fig. 10. The qualitative vision is therefore that the hydrophilic clusters form shortcuts avoiding hydrophobic regions that are invaded when f is lower. This is qualitatively illustrated by the patterns shown in Fig. 9 (compare the patterns for f varying between 10% and 50%).

The effect of f on S_{dppc} becomes much more important in the range [70–100%]. We note from Fig. 10 (bottom inset), that the probability that an active inlet bond belongs to a hydrophilic percolating cluster becomes greater than 0.5 in this range of f. As can be seen from Fig. 14, increasing f in this range leads to drastically reducing the percolating defending phase saturation, but only for a sufficiently thick system. For a sufficiently thin system, a large saturation greater than for a purely hydrophobic system, for example, can be obtained, which is again somewhat counterintuitive.

D. Defending phase transport capacity (diffusive conductance)

The evolutions of the diffusive conductance depicted in Fig. 15(a) are in line with the results on the percolating defending phase saturations of the previous subsection: no

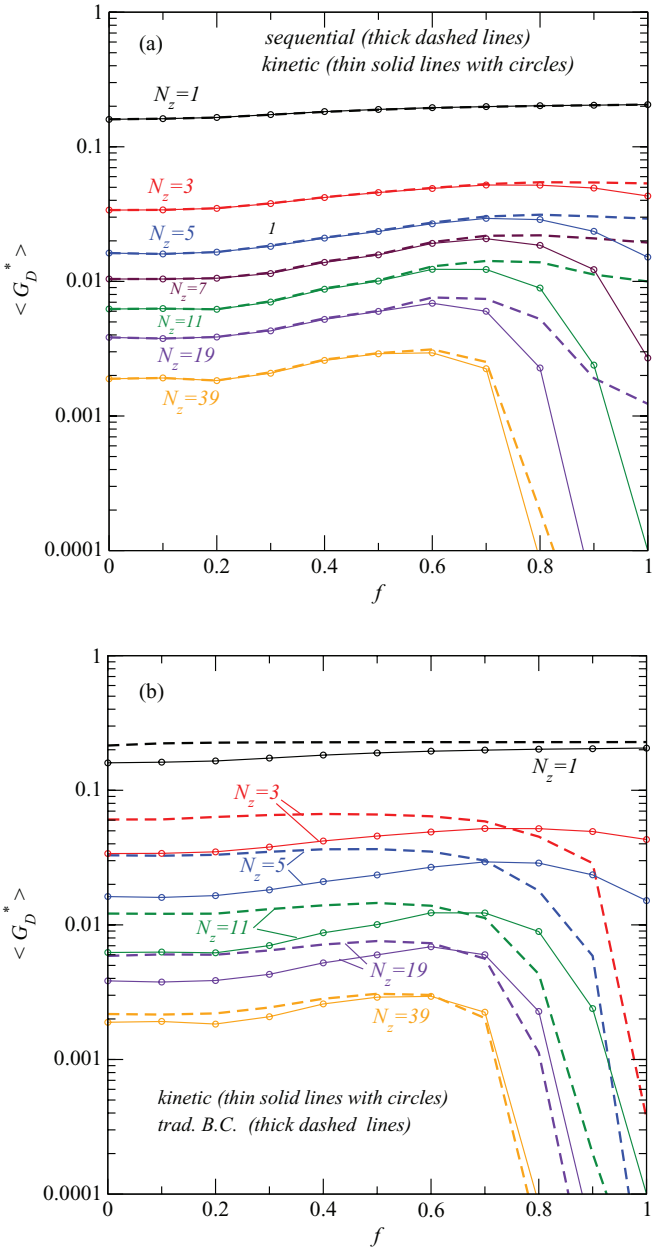

FIG. 15. (Color online) Variation of defending phase diffusive conductance G_D^* as a function of the fraction of hydrophilic elements for different system thicknesses (computed on $20 \times 20 \times N_z$ networks with $n_i = 10\%$). (a) kinetic and sequential flow scenarios, (b) comparison between the traditional boundary condition and the kinetic scenario.

influence of f on the results when $f \leqslant 20\%$; the conductance increases with f in the range [20%, 60%], which again, might appear as somewhat counterintuitive. For a given value of f, the conductance is greater in thin systems ($N_z < 10$) and decreases significantly with increasing N_z. Again, the differences between the sequential and kinetic invasions are marked only for $f > 60\%$, where the detrimental effect due to the increase in the hydrophilicity is much more marked when the invasion is sequential.

As can be seen from Fig. 15(b), the results are somewhat different with the traditional boundary condition when $f < f_c$. For a given thickness, $\langle S \rangle$ does not vary significantly with f as long as $f \leqslant f_c$ and increases rapidly with f for $f \geqslant f_c$ [see Fig. 13(b)]. As a result, G_D^* does not change significantly with f as long as as $f \leqslant f_c$ and decreases rapidly with f for $f \geqslant f_c$.

Hence, using the traditional boundary condition leads to an overestimation of the diffusive conductance for a given thickness when $f \leqslant f_c$ whereas the contrary is observed when $f > f_c$, especially when compared to the kinetic invasion. When the system becomes thick ($N_z = 39$ in Fig. 15), the traditional BC and the multiple injection kinetic and sequential invasions lead to much closer results, indicating that the system forgets the injection boundary condition when sufficiently thick. This is a consequence of the cluster coalescence mechanism.

As mentioned before, it is customary to characterize the diffusion transport through the concept of global apparent diffusion coefficient D^* ($\frac{D^*}{D} = N_z G_D^*$), with, very often in the literature, confusion between the apparent coefficient (characterizing the whole layer) and the effective coefficient (pertinent when the system is thick and the length separation sufficient). Also, it is generally assumed, although often implicitly or not clearly, that the apparent coefficient depends only on the microstructure and the saturation, i.e., is independent of the layer thickness N_z. As already discussed in Sec. III (see Fig. 7), this is wrong in a thin system because of the lack of length separation and the effect of the distribution of the fluids, which varies with the thickness. This is further illustrated in Fig. 16, which clearly shows that a one-to-one dependence of D^*/D with S cannot be expected in a thin system when the system is sufficiently hydrophobic ($f < 0.7$). To construct Fig. 16, we have computed $D^*(N_z, f)/D$ and S $(N_z, , f)$ varying N_z in the range [1, 20] and f in the range [0, 1] and then plotted $D^*(N_z, f)/D$ as a function of $S(N_z, f)$. Another interesting result shown in Fig. 16 is that the evolution of D^* with S is quite sensitive to the degree of hydrophilicity of the layer. This, together with the possible statistical fluctuations (see next subsection), can explain the difficulties encountered to experimentally characterize D^* for a partially wet thin system.

E. Statistical fluctuations

Again, statistical fluctuations can be noticeable (the standard deviation can be on the order of 10% of the mean value or even more) and this is illustrated in Fig. 17. As can be seen, the standard deviation of the conductance does not change significantly with f (except when the system is ultrathin, i.e., $N_z < 5$ in Fig. 17) as long as $f < f_c$. Also the fluctuations are identical with the sequential and the kinetic algorithms in

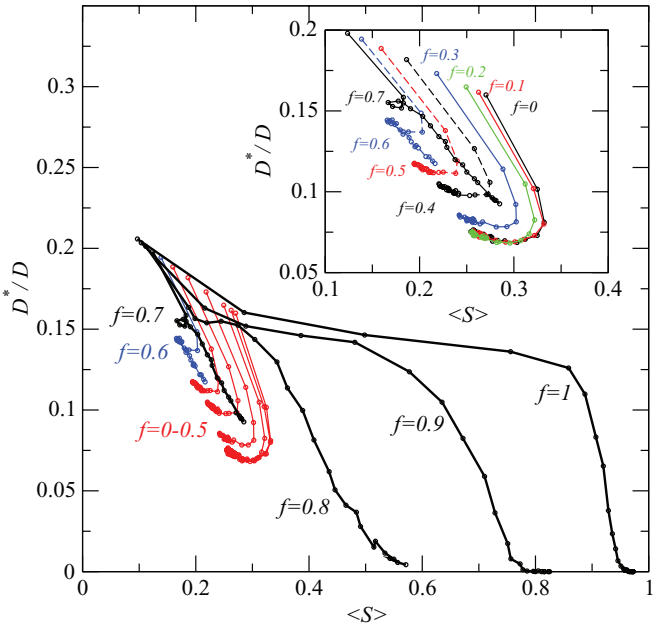

FIG. 16. (Color online) Variation of defending phase apparent diffusion coefficient as a function of invading phase saturation for different fractions of hydrophilic elements and various system thicknesses (see text). Results are for $20 \times 20 \times N_z$ networks with $n_i = 10\%$. The inset shows a detailed view for the hydrophilic element fractions in the range [0–0.7].

this range of f. Differences between the two invasion modes appear when $f > f_c$. As can be seen the standard deviation can increase significantly when $f > f_c$ when the invasion is kinetic. As noted in Sec. III D, the statistical fluctuations are expected to die out when $N_x \gg N_z$.

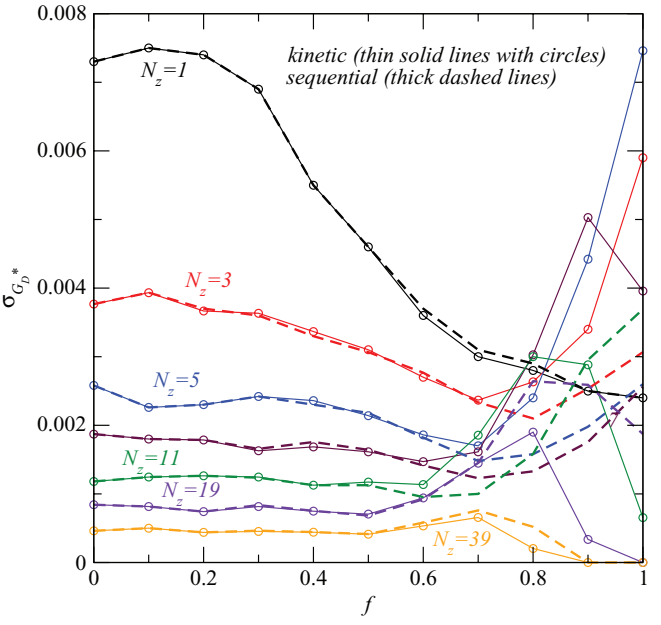

FIG. 17. (Color online) Variation of defending phase diffusive conductance standard deviation as a function of the fraction of hydrophilic elements for the two flow scenarios (computed on $20 \times 20 \times N_z$ networks with $n_i = 10\%$).

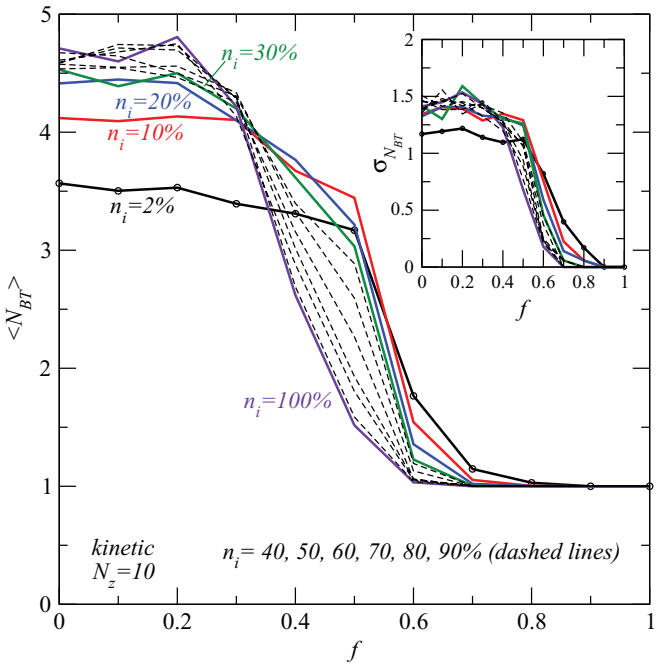

FIG. 18. (Color online) Probability that an outlet bond is a breakthrough point as a function of the fraction of hydrophilic elements for various fractions of active bonds n_i in a thin system ($N_z = 10$). Results are for $20 \times 20 \times N_z$ networks and the kinetic flow scenario. The inset shows the variation of the standard deviation of $N_{\rm BT}$.

F. Influence of n_i in a thin system

All the results presented so far in this section as regards the pore occupancy and the diffusive conductance were for a fraction of active inlet injection bonds of 10% ($n_i = 10\%$). In this section, we briefly look at the influence of f and n_i for a given thickness ($N_z = 10$). Also, for simplicity, we consider in this subsection only the results obtained with the kinetic algorithm (we recall in passing that the kinetic and sequential algorithms lead to the same results when $f < f_c$). As a representative example, we only present the variation of the number of breakthrough points as functions of n_i and f. The behavior of other quantities of interest, such as the defending phase diffusive conductance can be qualitatively inferred from the findings reported in the article. As can be seen from Fig. 18, the global evolution is similar whatever the value of n_i. Three main regions can be distinguished: (i) $\langle N_{\rm BT}\rangle$ does not depend on f provided that $f < 0.2$, (ii) $\langle N_{\rm BT}\rangle$ tends rapidly to 1 for f above f_c, (iii) the transition region between the two aforementioned regions, which shifts to the left as n_i increases. As shown in the inset in Fig. 18, the order of magnitude of the statistical fluctuations is not very sensitive to n_i.

V. APPLICATIONS TO PEMFC

As for [1], a motivation for the present work comes from the study of two-phase flows in the gas diffusion layer (GDL), e.g., [20–25], of proton exchange membrane fuel cells (PEMFCs), e.g., [21]; see also Sec. 5 in [1] for a short presentation of PEMFC. A GDL is a porous structure, whose thickness typically varies between 170 and 400 μm [20]. The lateral extension of a GDL is on the order of 10 cm. The thickness of a GDL is therefore about three orders of magnitude smaller that its lateral extension. The pore sizes in GDL range from a few microns to tens of microns and, as discussed, for example, in [26], the mean distance between two pores (referred to as the lattice spacing a later in the paper) is about 50 μm. Hence the GDL thickness measured in lattice spacing units is only 4–10. As pointed out in [1] a GDL is a perfect example of a thin porous system.

A GDL is generally treated with a hydrophobic fluoropolymer so as to render it hydrophobic on the grounds that this improves the PEMFC performances. This has to do with the so-called water management problem of PEMFC, which can be roughly described as follows; see [21] for more details. Water that forms in the catalyst layer (a porous layer adjacent to the GDL at the inlet) should be transported through the GDL without blocking the gas transport across the GDL. Hence roughly, as far as the GDL is concerned, the problem is to evacuate through the GDL the water that forms in excess in the catalyst layer while minimizing the impact of liquid water in the pores of the GDL on the gas access to the catalyst layer.

As discussed in [27], water invasion in a hydrophobic porous medium in the quasistatic limit that is expected to prevail for flows in fuel cells leads to capillary fingering whereas the invasion pattern is compact in a hydrophilic medium. The capillary fingering pattern leaves many pores not invaded by the liquid and therefore available for the gas transport. In contrast, the compact invasion pattern rapidly blocks the gas transport across the GDL. This explains why a hydrophobic GDL is considered as a better option.

Nevertheless it is widely admitted that the hydrophobic treatment is not perfect [4,19] and there are strong suspicions that aging of the GDL leads to a loss in hydrophobicity of the GDL [19]. The GDL is thus a good example of a system of mixed wettability.

The reasons for considering a multiple injection scenario at the inlet of a GDL are discussed in [1] and therefore will not be repeated here; see also [22]. We simply summarize the main findings of the paper as regards the GDL-PEMFC two-phase flow problem:

(1) The number of droplets forming at the surface of an operating GDL for a given number of injection points is highly dependent of the wettability of the GDL and the presence or not of trapping phenomena. Interestingly, since the exponent of the power law regions (see Fig. 12) depends on the wettability (and trapping) condition, the experimental determination of droplet density at the GDL outlet (by varying the number of injection points in a dedicated setup) could be an interesting and simple way of characterizing the wettability properties of GDLs. This type of measurement could be also exploited to characterize the aging of a GDL.

(2) As illustrated in this paper, there is not a one-to-one relationship between the apparent diffusion coefficient of a GDL and the liquid saturation. The apparent diffusion coefficient also depends on the thickness of the GDL. This puts into question the relevance of many previous numerical works assuming simply a classical one-to-one dependence between the apparent coefficient (furthermore often confused with an effective diffusion coefficient) and the liquid saturation.

(3) The properties of a partially water saturated GDL as regards the transport of gas by diffusion are highly dependent on the wettability properties. Hence the apparent diffusion coefficient also depends on the wettability properties (the fraction of hydrophilic elements in our approach). However, the dependence is marked only when the fraction of hydrophilic pores is greater than a critical value (denoted by f_c in the paper). This can be related to the aging problem of PEFMC. It is surmised [19] that the aging problem of PEMFC, i.e., the loss of performance during the operation of PEMFC, is due in part to the change in wettability of the GDL. According to our simulations, the system will not be sensitive to the loss of the hydrophobic coating as long as the fraction of hydrophilic elements is lower than f_c, whereas the system would become quite sensitive to this loss above f_c. This would nicely explain why the aging problem is not progressive but only occurs after a certain time.

(4) The traditional boundary condition ("adjacent reservoir BC") used frequently in the PEMFC literature leads to results markedly different from the multiple injection BC. For example, using the traditional boundary condition for a hydrophobic system leads to significantly overestimating the defending phase diffusive conductance except only when the fraction of active injection bonds at the inlet is quite low, on the order of 1–2%. According to the current understanding of two-phase flows in an operating GDL, the traditional BC should not be used anymore for the study of two-phase flows in GDL.

(5) Trapping phenomena can greatly affect the gas access. Trapping phenomena have been neglected so far in most GDL related pore network studies. A GDL is generally a fibrous material of relatively high porosity. Thus, it is quite possible that neglecting trapping phenomena is acceptable. This, however, remains to be proved. However, the GDL is often used in conjunction with a microporous layer (MPL) located at the inlet of the GDL, e.g., [20]. The MPL is much closer to a packing of microspheres. Thus, trapping phenomena could be significant in the MPL. Our results suggest that the possible effect of trapping phenomena should be systematically considered in analyzing two-phase flows in GDL and especially MPL-GDL assembly.

(6) In disagreement with many previous works published in relation with the study of PEMFC, our results show that applying the porous media traditional continuum approach to the modeling of transport phenomena in GDL leads to very poor approximations of the transport phenomena. This is due to the lack of length scale separation characteristic of thin systems and to the scale dependence of flow path coalescence phenomena, which lead to scale dependent results.

VI. CONCLUSIONS

Thin porous media can be considered as a distinct class of porous media. However, it is not necessarily easy to know in advance when a porous medium can be defined as thin. This notably depends on the particular transport phenomenon considered. However, the fact that the transport properties are scale dependent—that is, they depend on the thickness—can be considered as a generic characteristic of thin systems.

This was well illustrated through the specific process considered in this study: the quasistatic displacement of a wetting fluid by a nonwetting fluid in a porous layer with multiple independent injection points at the inlet. In this example, the behavior of sufficiently thin porous media is distinct from that of thicker porous media. The average number of breakthrough points varies as a function of the system thickness for a sufficiently thin porous medium. By contrast this number becomes independent of the system thickness when the system is sufficiently thick. Our results also reveal that the behavior of ultrathin systems is different from thicker thin systems. The number of breakthrough points varies according to a power law in a sufficiently thick, not too hydrophilic thin system whereas the variation is different for an ultrathin porous medium, slower than the power law scaling, and not described by a power law behavior.

The exponent of the power law and the fluid distribution at the end of the displacement are independent of the flow scenario, sequential or kinetic, when the system is fully hydrophobic (that is, the invading fluid is everywhere nonwetting) and when trapping is negligible. By contrast, this does not hold anymore in the presence of trapping or in systems of mixed wettability.

The thickness marking the beginning of the power law region depends on the significance of trapping and on the wettability properties. For example, the aforementioned power law behavior is observed for thinner systems when trapping is perfect or the fraction of hydrophilic pores is above the hydrophilic pore percolation threshold.

The fact that the properties are scale dependent in a thin system was also well illustrated through the study of the defending phase transport properties. Contrary to what was generally assumed in many previous works, there is not a one-to-one relationship between the overall diffusive conductance and the mean saturation in a thin system. The diffusive conductance depends on the system thickness.

The findings of this paper were finally discussed in relation with the so-called water management problem in proton exchange membrane fuel cells (PEMFCs). The optimization of PEMFC clearly needs a better understanding of the physics involved in this technology. PEMFC can thus be regarded both as an object of great technological importance and as a source of interesting scientific problems.

ACKNOWLEDGMENTS

Financial support from GIP ANR (Project No. ANR-06-PANH-022-02 "Chameau"), CEA, and CNRS are gratefully acknowledged.

[1] L. Ceballos, M. Prat, and P. Duru, Phys. Rev. E **84**, 056311 (2011).

[2] D. Wilkinson and J. F. Willemsen, J. Phys. A **16**, 3365 (1983).

[3] M. J. Blunt and H. Scher, Phys. Rev. E **52**, 6387 (1995).

[4] J. D. Fairweather, P. Cheung, and D. T. Schwartz, J. Power Sources **195**, 787 (2010).

[5] P. Ustohal, F. Stauffer, and T. Dracos, J. Contam. Hydrol. **33**, 5 (1998).

[6] D. Zhou and M. Blunt, J. Pet. Sci. Eng. **20**, 203 (1998); M. Piri and M. J. Blunt, Phys. Rev. E **71**, 026301 (2005).

[7] V. Joekar-Niasar, S. M. Hassanizadeh, and H. K. Dahle, J. Fluid. Mech. **655**, 38 (2010)

[8] R. Lenormand and C. Zarcone, in *Proceedings of the 59th Annual Technical Conference of the Society of Petroleum Emgineers of AIME, Houston, 1984* (American Institute of Mining, Metallurgical, and Petroleum Engineers, Richardson, TX, 1984), Paper 13264; M. Cieplak and M. O. Robbins, Phys. Rev. B **41**, 11508 (1990); N. Martys, M. Cieplak, and M. O. Robbins, Phys. Rev. Lett. **66**, 1058 (1991); O. Chapuis and M. Prat, Phys. Rev. E **75**, 046311 (2007).

[9] V. Mani and K. K. Mohanty, J. Pet. Sci. Eng. **23**, 173 (1999).

[10] M. J. Blunt, Soc. Pet. Eng. J. **2**, 449 (1997); J. Pet. Sci. Eng. **20**, 117 (1998).

[11] L. Ceballos, Ph.D. thesis, INP. Toulouse, 2011.

[12] J. Bear, *Dynamics of Fluids in Porous Media* (Dover Publications, Inc., New York, 1988); J. H. Kim, A. Ochoa, and S. Whitaker, Transp. Porous Media **2**, 327 (1987).

[13] P. Moldrup, T. Olesen, S. Komatsu, P. Schjønning, and D. E. Rolston, Soil Sci. Soc. Am. J. **65**, 613 (2001).

[14] J. L. Auriault, Int. J. Eng. Sci. **29**, 785 (1991).

[15] M. Prat, Int. J. Multiphase Flow **19**, 691 (1993).

[16] J. T. Gostick, M. A. Ioannidis, M. W. Fowler, and M. D. Pritzker, J. Power Sources **173**, 277 (2007).

[17] S. Whitaker, *The Method of Volume Averaging* (Kluwer Academic Publishers, Dordrecht, 1999).

[18] D. A. G. Bruggeman, Ann. Phys. **24**, 636 (1935).

[19] S. Pulloor Kuttanikkad, M. Prat, and J. Pauchet, J. Power Sources **196**, 1145 (2011).

[20] P. P. Mukherjee, Q. Kang, and C. Y. Wang, Energy Environ. Sci. **4**, 346 (2011); S. Park, J.-W. Lee, and B. N. Popov, Int. J. Hydrogen Energy **37**, 5850 (2012).

[21] F. Barbir, *PEM Fuel Cells: Theory and Practice* (Elsevier Academic Press, New York, 2005); M. Eikerling, A. A. Kornyshev, and A. R. Kucernak, Phys. Today **59**(10), 38 (2006); Y. Wang, K. S. Chen, J. Mishler, S. C. Cho, and X. C. Adroher, Appl. Energy **88**, 981 (2011).

[22] K. J. Lee, J. H. Nam, and C. J. Kim, Electrochim. Acta **54**, 1166 (2009).

[23] L. Chen, H.-B. Luan, Y.-L. He, and W.-Q. Tao, Int. J. Therm. Sci. **51**, 132 (2012).

[24] J. H. Nam and M. Kaviany, Int. J. Heat Mass Transfer **46**, 4595 (2003).

[25] P. K. Sinha, P. P. Mukherjee, and C. Y. Wang, J. Mater. Chem. **17**, 3089 (2007).

[26] M. Rebai and M. Prat, J. Power Sources **192**, 534 (2009).

[27] O. Chapuis, M. Prat, M. Quintard, E. Chane-Kane, O. Guillot, and N. Mayer, J. Power Sources **178**, 258 (2008).